

## SOFT ROBOTS

## Inflatable soft jumper inspired by shell snapping

Benjamin Gorissen<sup>1\*</sup>, David Melancon<sup>1\*</sup>, Nikolaos Vasilos<sup>1</sup>, Mehdi Torbati<sup>1</sup>, Katia Bertoldi<sup>1,2,3†</sup>

Fluidic soft actuators are enlarging the robotics toolbox by providing flexible elements that can display highly complex deformations. Although these actuators are adaptable and inherently safe, their actuation speed is typically slow because the influx of fluid is limited by viscous forces. To overcome this limitation and realize soft actuators capable of rapid movements, we focused on spherical caps that exhibit isochoric snapping when pressurized under volume-controlled conditions. First, we noted that this snap-through instability leads to both a sudden release of energy and a fast cap displacement. Inspired by these findings, we investigated the response of actuators that comprise such spherical caps as building blocks and observed the same isochoric snapping mechanism upon inflation. Last, we demonstrated that this instability can be exploited to make these actuators jump even when inflated at a slow rate. Our study provides the foundation for the design of an emerging class of fluidic soft devices that can convert a slow input signal into a fast output deformation.

## INTRODUCTION

Inflatable soft actuators have emerged as an ideal platform to realize active structures capable of safe interactions with unstructured environments (1–3). Their compliance and ability to achieve complex deformations has enabled the design of flexible machines for a wide spectrum of applications (4), ranging from minimally invasive surgical tools (5) and exoskeletons (6) to warehouse grippers (7) and add-ons for video games (8). However, existing fluidic soft actuators are typically slow, because a substantial amount of fluid has to be supplied for their operation, the influx of which is restricted by viscous forces in tubes and valves. To overcome this limitation, it has been shown that fast actuation can be achieved either by modifying the geometry to reduce the amount of fluid needed for inflation (9) or by using chemical reactions to generate explosive bursts of pressure (10). Alternatively, snapping instabilities can also provide a powerful nonlinear mechanism that decouples the slow input signal from the output deformation and triggers rapid events (11–15).

Inspired by recent progress using snapping instabilities to increase the speed of actuation (11, 16), we investigated the snapping of spherical caps as a mechanism to realize fluidic soft actuators capable of rapid movements. We first showed that the snapping of elastomeric spherical caps upon pressurization results in a sudden release of energy, the amount of which can be controlled by tuning the caps' geometry, material stiffness, and boundary conditions at the edges. We then realized fluidic soft actuators by combining two spherical caps (see Fig. 1A) and found that the energy released upon snapping of the inner cap leads to a rapid inversion of its pole that ultimately enables jumping. Last, we identified geometric and material parameters that result in substantial energy release and jump height, providing a rich design domain for fluidic soft actuators capable of extremely fast movements regardless of inflation rate.

## RESULTS

## Snapping of spherical caps as a platform for fast fluidic soft robots

To create fast inflatable soft actuators, we started by conducting finite element (FE) analyses to investigate the response upon pressurization of elastomeric spherical caps with radius,  $R$ , thickness,  $t$ , and polar angle,  $\theta$  (see Fig. 1B). In our simulations (which were conducted using the commercial package ABAQUS 2018/Standard), we assumed the deformation to be axisymmetric, discretized the models with four-node bilinear axisymmetric solid elements, and used an incompressible Gent material model with initial shear modulus,  $\mu$  (17). We pressurized the caps by supplying incompressible fluid to a cavity above them (highlighted in gray in the inset in Fig. 1B) and simulated the quasi-static pressure-volume curve via the modified Riks algorithm (18, 19). In Fig. 1B, we consider a thin cap with polar angle  $\theta = 60^\circ$ , normalized radius  $\eta = R/t = 30$ , and clamped boundary conditions at the base. We found that the pressure-volume curve of this cap is qualitatively identical to those recently reported for pressurized spherical shells (20–22) and is characterized by a limit point when inflating under volume-controlled conditions (indicated by a black circular marker in Fig. 1B). This volume limit causes an instability, leading the system to snap to a point of lower pressure (white circular marker in Fig. 1B). This occurs while conserving the volume in the cavity and results in a partial inversion of the cap, which we characterize by quantifying the distance traveled by the pole during the instability,  $\Delta y_{\text{pole}}$  (see insets in Fig. 1B). Further, we note that the isochoric snapping of the cap is accompanied by a sudden release of energy,  $\Delta E$ , that graphically corresponds to the green highlighted area in Fig. 1B and can be obtained as

$$\Delta E = \int_{\Gamma} p \, d\Delta V \quad (1)$$

where  $\Gamma$  is the equilibrium path that connects the limit point in volume and the corresponding isochoric point on the lower branch (highlighted by a dashed black line in Fig. 1B). For the considered cap, we find  $\Delta E = 1.50 \times 10^{-5} \mu R^3$  and  $\Delta y_{\text{pole}} = 1.31 \times 10^{-1} R$ .

Next, to investigate the effect of geometry on  $\Delta E$  and  $\Delta y_{\text{pole}}$ , we compared the response of the thin spherical cap with that of a thicker one with  $\eta = 8.5$  and both with clamped and roller boundary conditions at the base. The results reported in Fig. 1C indicate that the

<sup>1</sup>J.A. Paulson School of Engineering and Applied Sciences, Harvard University, Cambridge, MA 02138, USA. <sup>2</sup>Wyss Institute for Biologically Inspired Engineering, Harvard University, Cambridge, MA 02138, USA. <sup>3</sup>Kavli Institute for Bionano Science and Technology, Harvard University, Cambridge, MA 02138, USA.

\*These authors contributed equally to this work.

†Corresponding author. Email: bertoldi@seas.harvard.edu

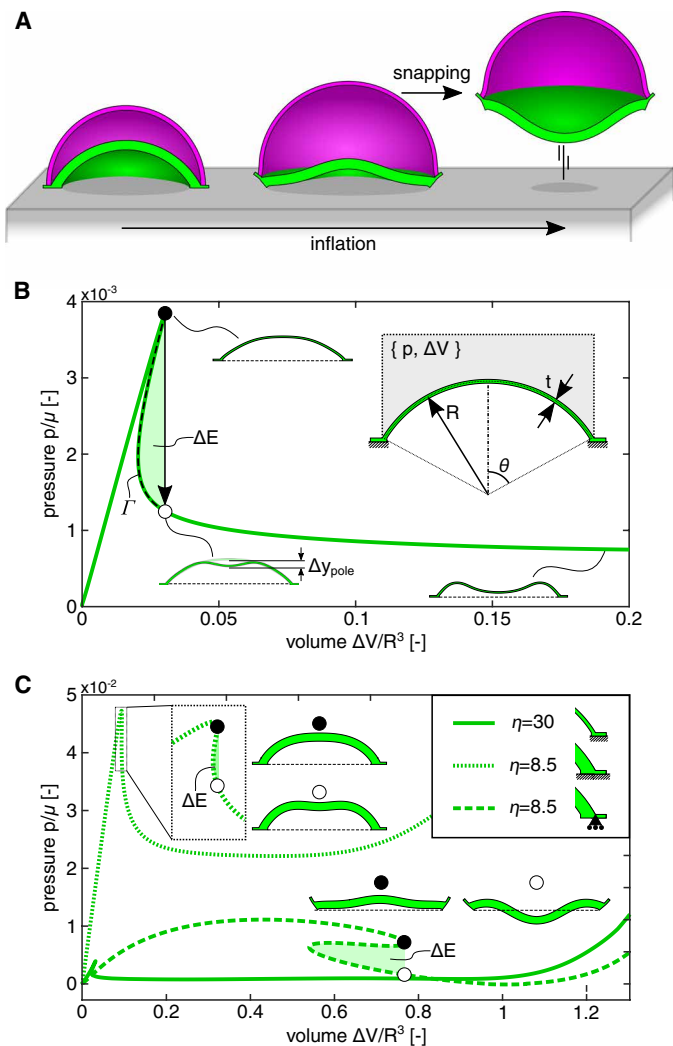


**Fig. 1. Snapping of spherical caps for fast fluidic soft robots.** (A) Our soft fluidic actuators comprise two spherical caps connected at their base. Upon inflation, the inner cap snaps and enables our simple device to take off. (B) The pressure-volume curve, normalized by initial shear modulus,  $\mu$ , and radius,  $R$ , of a given pressurized spherical cap is characterized by a limit point when inflating under volume-controlled conditions. This volume limit point causes an isochoric snapping instability, which leads to a sudden release of energy,  $\Delta E$  (highlighted in green), and the inversion of the inner cap (which we characterize by quantifying the distance travelled by the cap's pole,  $\Delta y_{\text{pole}}$ ). (C) Comparison between the pressure-volume curves of thin (solid green line) and thick spherical caps with both clamped (dotted green line) and roller (dashed green line) boundary conditions. Note that the normalized radius  $\eta$  is defined as the ratio of cap radius over cap thickness (i.e.,  $\eta = R/t$ ).

boundary conditions play a major role on the snapping behavior. The clamped thick cap is characterized by a very large maximum pressure, but a very small energy release and pole displacement upon snapping ( $\Delta E = 4.78 \times 10^{-6} \mu R^3$  and  $\Delta y_{\text{pole}} = 6.30 \times 10^{-2} R$ ). On the other hand, roller boundary conditions lower the maximum pressure but lead to a much higher energy release and pole displacement ( $\Delta E = 8.00 \times 10^{-4} \mu R^3$  and  $\Delta y_{\text{pole}} = 2.67 \times 10^{-1} R$ ). As a result, our simulations indicate not only that isochoric snapping of spherical caps provides opportunities to realize systems capable of suddenly releasing a substantial amount of energy through their

inversion but also that by tuning geometry and boundary conditions, we can control and maximize the response of these systems.

### Inflatable soft actuators inspired by shell snapping

Having demonstrated numerically that snapping of a spherical cap results in a sudden energy release and pole displacement, we then investigated the mechanical response of fully soft actuators comprising two spherical caps connected at their base to form a cavity that we inflate with an incompressible fluid (see Fig. 1A). We began by considering three actuators with inner caps identical to those introduced in Fig. 1C (with  $R_i = 30$  mm) with outer caps characterized by  $\theta_o = 90^\circ$  and  $\eta_o = 16.5$  (note that here and in the following, the subscripts o and i are used to indicate properties of the outer and inner caps, respectively). Specifically, design A has a thin inner cap with  $\theta_i = 60^\circ$  and  $\eta_i = 30$ , whereas designs B and C have a thick cap with  $\theta_i = 60^\circ$  and  $\eta_i = 8.5$ . Further, we assumed that both caps of designs A and B are made of the same elastomeric material (i.e.,  $\mu_i/\mu_o = 1$ ); however, for design C, we consider an outer cap made of a softer rubber, resulting in  $\mu_i/\mu_o = 5.8$ . The numerically obtained pressure-volume curves for the three actuators (shown in Fig. 2A as blue lines) share many features with those reported in Fig. 1C for the individual pressurized caps and are all characterized by a limit point near the maximum pressure when considering volume-controlled conditions. Hence, our actuators also exhibit isochoric snapping upon inflation, and this again results in a sudden release of elastic energy and the inversion of the inner cap. By comparing the responses of the three actuators, we find that design C exhibits the largest energy release and displacement of the inner cap's pole ( $\Delta E = 0.875, 5.67$ , and  $31.4$  mJ for designs A, B, and C, respectively, whereas  $\Delta y_{\text{pole}} = 7.68, 7.55$ , and  $20.89$  mm for designs A, B, and C, respectively). These results agree with the trends observed for the individual pressurized caps (see Fig. 1C), because both  $\Delta E$  and  $\Delta y_{\text{pole}}$  increase for thicker caps that are allowed to rotate at their base (note that in our actuators, such boundary conditions are not directly controlled but rather determined by the outer cap; see fig. S13). Furthermore, the results highlight the important role of the outer caps and indicate that both  $\Delta E$  and  $\Delta y_{\text{pole}}$  can be enhanced by increasing their compliance. This is because compliant outer caps can sustain more deformation before snapping (see insets in Fig. 2A) and, therefore, enable the actuator to store more elastic energy that can be potentially released upon instability.

Next, to experimentally validate our analyses, we fabricated the three actuators using molds and inflated them with water while submerged in water to eliminate the effects of gravity (see the Supplementary Materials for details). In this experimental analysis, all caps were fabricated out of Zhermack Elite Double 32 (with green color and initial shear modulus  $\mu = 0.35$  MPa), except for the outer cap of design C, where we used Zhermack Elite Double 8 (with purple color and initial shear modulus  $\mu = 0.06$  MPa). Note that these values were obtained by minimizing the error between experiments and simulations for design C and are within the range previously reported in the literature (21, 23–25). In Fig. 2A, we compare the numerical (blue lines) and experimental (red lines) pressure-volume curves for the three actuators, whereas in Fig. 2B, we display snapshots that are taken during the tests. We found good agreement between simulations and experiments, with pressure measurements that show a sudden drop near the numerically predicted limit point. The small discrepancies between experiments and simulations can be attributed to unavoidable imperfections introduced during fabrication,

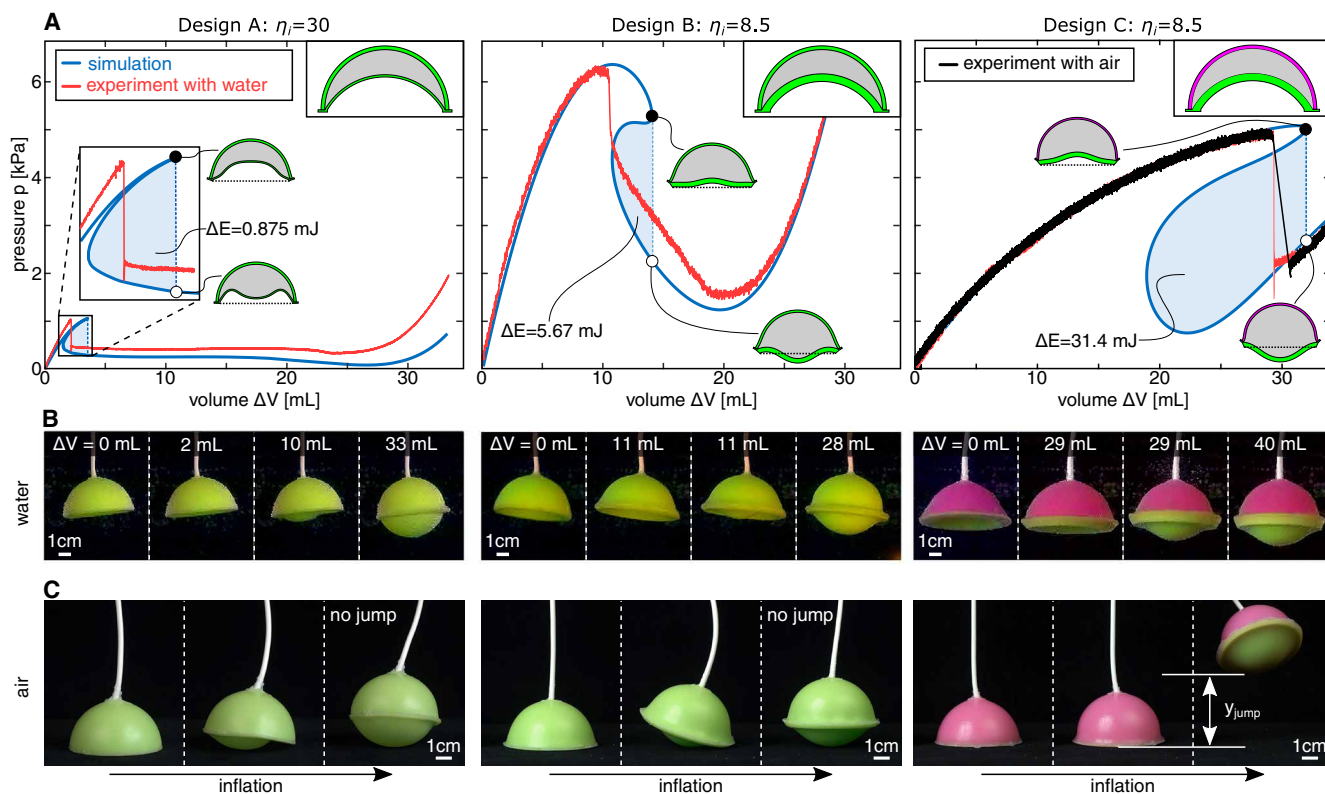


**Fig. 2. Our inflatable soft actuators.** (A) Experimental (red) and numerical (blue) pressure-volume curves for the inflation with water of three actuators (all with inner cap radius  $R_i = 30$  mm) characterized by normalized radii, polar angles, and ratio of shear moduli  $(\eta_i, \theta_i, \eta_o, \theta_o, \mu_i/\mu_o) = (30, 60^\circ, 16.5, 90^\circ, 1)$  (design A),  $(8.5, 60^\circ, 16.5, 90^\circ, 1)$  (design B), and  $(8.5, 60^\circ, 16.5, 90^\circ, 5.8)$  (design C). The energy released upon snapping,  $\Delta E$ , is highlighted by the shaded blue region. The volume limit point upon inflation is identified with a black circular marker, whereas its corresponding isochoric point on the lower branch is identified with a white circular marker. For design C, we also report the experimental pressure-volume curve obtained when inflating the actuator with air (black line). (B) Experimental snapshots of the three design during inflation with water at different amounts of supplied fluid. (C) Experimental snapshots of the three designs during inflation with air. The isochoric snapping makes design C jump and reach a maximum height denoted  $y_{\text{jump}}$ .

visco-elasticity of the rubber, and slight asymmetric buckling of the inner cap. Furthermore, in all of our tests, as observed in the simulations, snapping is also accompanied by the sudden inversion of the inner cap. For design A,  $\Delta y_{\text{pole}}$  is such that the inner cap's pole remains above the base plane of the actuator upon snapping; for designs B and C, however, the large value of  $\Delta y_{\text{pole}}$  allows for their inner cap's pole to cross it (see Fig. 2B).

Motivated by these results, we investigated how snapping can be exploited to enhance the functionality of our simple robots and to make them jump even when inflated at a slow rate. To this end, we positioned our actuators on a flat surface and slowly inflated them with air (see the Supplementary Materials for details). The snapshots reported in Fig. 2C reveal that, despite the slow rate of inflation (10 ml/min with a syringe pump), the isochoric snapping makes design C jump and reach a maximum height of  $y_{\text{jump}} = 42.9$  mm. On the other hand, although the inner cap of designs A and B snaps upon inflation, their  $\Delta E$  and  $\Delta y_{\text{pole}}$  are not large enough to enable them to take off. Although this last set of tests was conducted using a compressible fluid (air), the effect of fluid compressibility on the response of the system's energy release was negligible and only led to a slight increase of volume during snap-through (see Fig. 2A and the Supplementary Materials for details). Hence, the experiments and analyses conducted using an incompressible fluid can be also used to understand and improve the performance of our air-inflated jumpers.

### Improving the actuators' response

Thus far, we have shown that the geometry and material properties of the caps strongly affect the snapping behavior and that by tuning  $\Delta E$  and  $\Delta y_{\text{pole}}$ , we can harness the instability to make our actuators jump. Motivated by these findings, we proceeded by systematically exploring the parameter space to identify designs that can jump higher than design C. Figure 2C indicates that jumping requires large enough  $\Delta E$  and  $\Delta y_{\text{pole}}$ , and Fig. 2A indicates that  $\Delta E$  and  $\Delta y_{\text{pole}}$  can be enhanced by combining an inner cap that releases a large amount of energy upon snapping with an outer cap that stores a large amount of energy before snapping. Therefore, we started by considering the two caps separately and used axisymmetric FE analyses to investigate their behavior for a wide range of geometric parameters (i.e.,  $40^\circ \leq \theta_i \leq 80^\circ$ ,  $5 \leq \eta_i \leq 12.5$ ,  $40^\circ \leq \theta_o \leq 90^\circ$ , and  $5 \leq \eta_o \leq 20$ ).

Focusing on the inner cap, we found that by varying  $\theta_i$  and  $\eta_i$ , its response undergoes several transitions (see Fig. 3, A and B). For low values of  $\theta_i$  and  $\eta_i$  (i.e., for thick and shallow caps), the inner cap does not exhibit isochoric snapping (see light gray region in Fig. 3, A and B). By increasing  $\theta_i$  at constant  $\eta_i$ , snapping is eventually triggered upon inflation. Within this domain, both the energy released by the inner cap,  $\Delta E_i$ , and its pole displacement,  $\Delta y_{\text{pole}}$ , increase monotonically as a function of  $\theta_i$ , suggesting that the response of our actuators can be enhanced by considering deep and sufficiently thick inner caps. Last, for high values of  $\theta_i$  and  $\eta_i$  (i.e., for thin and deep caps), the

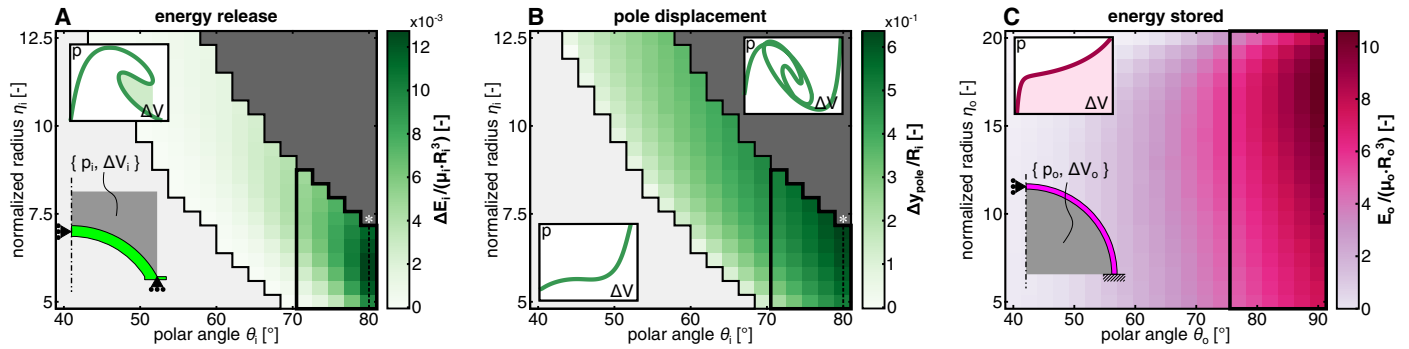


**Fig. 3. Mechanical response of the inner and outer caps upon inflation.** (A and B) Evolution of the inner cap's normalized (A) energy release,  $\Delta E_i / (\mu_i R_i^3)$ , and (B) pole displacement,  $\Delta y_{\text{pole}} / R_i$ , upon snapping as a function of the normalized radius,  $\eta_i$ , and the polar angle,  $\theta_i$ . (C) Evolution of the outer cap's normalized stored energy at  $p/\mu_o = 0.5$ ,  $E_o / (\mu_o R_o^3)$ , as a function of the normalized radius,  $\eta_o$ , and the polar angle,  $\theta_o$ .

pressure-volume curves become self-crossing (see dark gray region in Fig. 3, A and B), which is an indication of the existence of a more favorable asymmetric deformation path with low  $\Delta E_i$  and  $\Delta y_{\text{pole}}$  (see fig. S16).

Next, we turned our attention to the outer cap and found that its response is less rich and resembles that of an inflated thin spherical balloon (26, 27). Because the outer cap in our actuators acts as an energy reservoir, in Fig. 3C, we report the evolution of the stored energy in the outer cap,  $E_o$ , at a normalized pressure of  $p/\mu_o = 0.5$ , as a function of the polar angle,  $\theta_o$ , and the normalized radius,  $\eta_o$ . The results indicate that  $E_o$  increases monotonically with  $\theta_o$  (almost irrespective of  $\eta_o$ ), therefore suggesting that the response of our actuators can be enhanced by focusing on deep outer caps.

Although the results of Fig. 3 enabled us to identify promising regions of the design space (i.e., inner caps with  $\theta_i \geq 70^\circ$  and  $\eta_i \leq 8$  and outer ones with  $\theta_o \geq 76^\circ$ ), they could not be directly used to realize the best possible jumper because they neglect the coupling between the two caps. Therefore, as next step, we used axisymmetric FE analyses to simulate the response of 4800 actuators constructed by combining inner and outer caps within the identified promising regions (highlighted by black contours in Fig. 3). In Fig. 4A, we report  $\Delta E$  and  $\Delta y_{\text{pole}}$  for all simulated actuators with both  $\mu_i/\mu_o = 1$  (green markers) and 5.8 (purple markers). Four key features emerge from the plot. First, by comparing the results with those obtained for the three actuators considered in Fig. 2 (indicated by square markers in Fig. 4A), we find that both  $\Delta E$  and  $\Delta y_{\text{pole}}$  can be greatly increased when the geometry is properly tuned. Second, the results show that, on one hand, there is a strong correlation between  $\Delta E$  and  $\Delta y_{\text{pole}}$  and, on the other hand, there is a disconnection between them and the drop in pressure associated with the snapping instability. Specifically, by inspecting the pressure-volume curves for the actuators (shown as insets in Fig. 4A), we found that for the designs with large  $\Delta E$  and  $\Delta y_{\text{pole}}$ , the drop in pressure is small, whereas the area enclosed by the pressure-volume curve between the limit point and the corresponding isochoric point on the lower branch is large. Third, the results confirmed the importance of a flexible outer cap because both  $\Delta E$  and  $\Delta y_{\text{pole}}$  span a much larger domain for the actuators with  $\mu_i/\mu_o = 5.8$ . Fourth, we found that the inner cap plays a crucial role and that by choosing  $\theta_i = 80^\circ$  to optimize its response, we can further improve the performance of the actuators (see black contour markers in Fig. 4A). At the same time, however, the results also highlight that for actuators with  $\mu_i/\mu_o = 5.8$ , the outer cap

geometry is important, because some design choices lead to noticeably lower  $\Delta E$  and  $\Delta y_{\text{pole}}$ .

Our quasi-static FE simulations allowed us to efficiently explore the design space and calculate  $\Delta E$  and  $\Delta y_{\text{pole}}$  for a large number of designs. However, because they do not account for dynamic effects, they cannot be used to directly characterize the ability of the actuators to jump. To overcome this limitation, we established a simple mass-spring model that takes the FE results of Fig. 4A as input and predicts the jump height,  $y_{\text{jump}}$ . This reduced order model comprises two concentrated masses,  $m_i$  and  $m_o$ , connected by a spring with stiffness  $k_s$  and rest length  $L_0$  (Fig. 4B). We chose  $m_i$  and  $m_o$  to be equal to the mass of the inner and outer cap, respectively, and to be located at their corresponding poles. We then focused on the numerically predicted configurations immediately before and after snapping and assumed that the mechanical system stores an amount of energy equal to  $\Delta E$  in the former and is stress free in the latter. It follows that  $L_0$  is equal to the distance between the poles immediately before snapping and that (see Fig. 4B)

$$k_s = \frac{2\Delta E}{(\Delta y_{\text{pole}})^2}. \quad (2)$$

Last, we consider the spring to be initially precompressed by  $\Delta y_{\text{pole}}$  and  $m_i$  to be positioned at a distance  $h_{\text{imp}}$  from the ground ( $h_{\text{imp}}$  being the numerically predicted distance of the inner cap's pole from the ground immediately before snapping). At time  $t = 0$ , we released the system and analytically determined the position of the two masses,  $y_i(t)$  and  $y_o(t)$ , as a function of time while accounting for contact with a rigid surface.

To verify the validity of our simplified mass-spring model, we first focused on three designs with  $(\eta_i, \theta_i, \eta_o, \theta_o, \mu_i/\mu_o) = (8.5, 60^\circ, 16.5, 90^\circ, 5.8)$  (design C),  $(5.4, 80^\circ, 15.3, 87^\circ, 5.8)$ , and  $(5.8, 80^\circ, 10.5, 85^\circ, 5.8)$  and compared the experimentally measured jump heights ( $h_{\text{jump}} = 42.9, 160$ , and  $209$  mm, respectively) to the predicted ones. When choosing a coefficient of restitution  $\alpha = 0.5$  and approximating the effect of dissipation with a linear dashpot with damping coefficient  $c_d = 0.4$  kg/s, we found excellent agreement between the two sets of data, with the model predicting  $y_{\text{jump}} = \max(y_i(t)) = 41.4, 175$ , and  $226$  mm (see the Supplementary Materials for details). Hence, these results indicate that our simple mass-spring model, despite the fact that it cannot capture the complex dynamic behavior typical of shells (14, 28, 29), can accurately predict the jump height

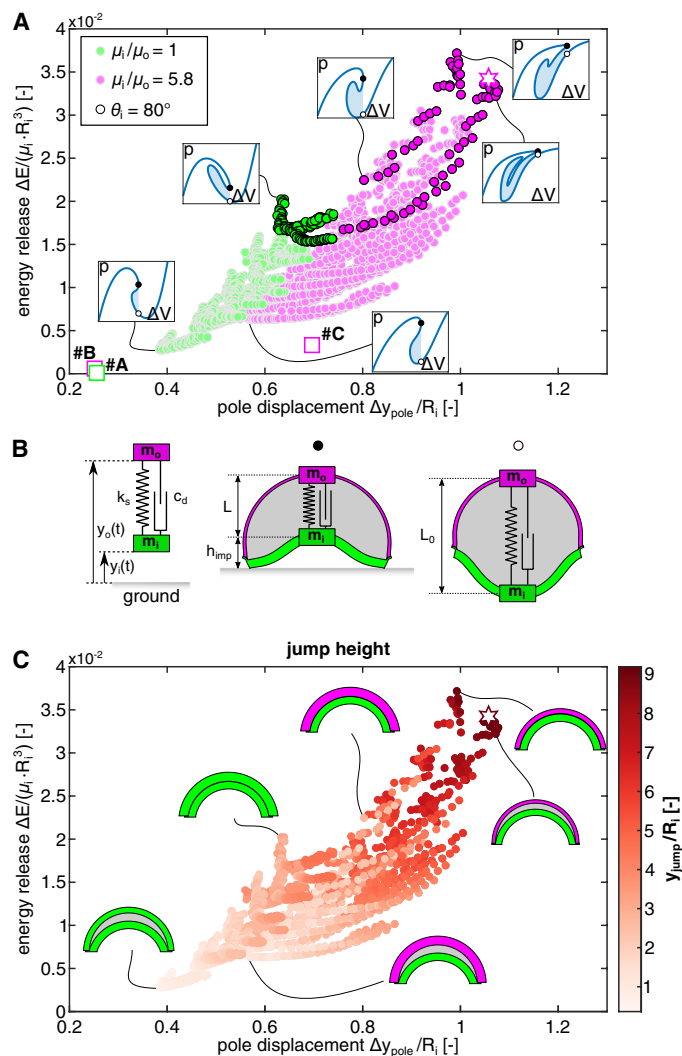


**Fig. 4. Improving the response of the actuators.** (A) Normalized energy release,  $\Delta E / (\mu_i R_i^3)$ , versus normalized pole displacement,  $\Delta y_{\text{pole}} / R_i$ , for actuators with inner polar angle  $\theta_i \geq 70^\circ$ , normalized inner radius  $\eta_i \leq 8$ , and normalized outer radius  $\theta_o \geq 76^\circ$ . (B) Reduced order mass-spring model used to predict jump height based on the numerical results reported in (A). The model comprises two masses  $m_i$  and  $m_o$  connected via a spring with stiffness  $k_s$  and a dashpot with damping coefficient  $c_d$ . (C) Normalized jump height,  $y_{\text{jump}} / R_i$ , as a function of energy release and pole displacement for the 4800 actuators considered in (A).

of our soft jumpers. Having confirmed the validity of our model, we then used it to calculate the  $y_{\text{jump}}$  for all 4800 actuators considered in Fig. 4A. The results reported in Fig. 4C indicate that a high jump requires both  $\Delta E$  and  $\Delta y_{\text{pole}}$  to be large. Specifically, we found that the jump height is highest for an actuator with  $(\eta_i, \theta_i, \eta_o, \theta_o, \mu_i / \mu_o) = (6.2, 80^\circ, 12.1, 82^\circ, 5.8)$  for which  $\Delta E = 324$  mJ and  $\Delta y_{\text{pole}} = 31.7$  mm. For such an actuator, our model predicts  $y_{\text{jump}} = 275$  mm, a jump height that is one order of magnitude larger than that previously recorded for design C. Our experimental results fully confirmed the numerical predictions for this design for both the pressure-volume curve (see Fig. 5A) and the jump height  $y_{\text{jump}} = 283$  mm (see Fig. 5B), further reinforcing the validity and efficiency of our numerical scheme to identify actuators with improved performance.

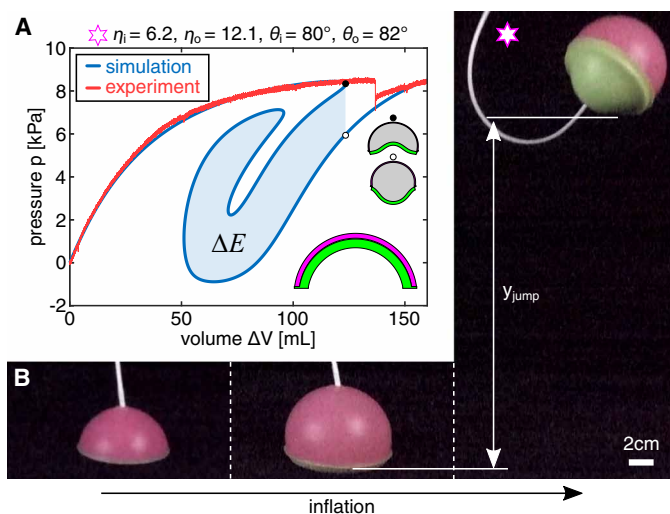


**Fig. 5. Actuator with highest jump height.** (A) Numerical (blue line) and experimental (red line) pressure-volume curves for the actuator with normalized radii, polar angles, and ratio of shear moduli  $(\eta_i, \theta_i, \eta_o, \theta_o, \mu_i / \mu_o) = (6.2, 80^\circ, 12.1, 82^\circ, 5.8)$  and inner cap radius  $R_i = 30$  mm. (B) Experimental snapshots of the actuator upon inflation with air.

## CONCLUSION

In summary, we have introduced a new family of inflatable soft actuators that harness isochoric snapping to move rapidly and even jump when inflated slowly. This behavior is encoded in their pressure-volume relationship, which exhibits two limit points in volume. Although fluidic actuators are typically characterized by a monotonic pressure-volume curve (9, 30), it has been recently shown that limit points in pressure can be exploited to enhance their functionality and enable sequencing (31–33). Here, we show that by introducing limit points in volume, we can realize soft robots capable of suddenly releasing a given amount of energy. Because the instability occurs at constant volume and does not involve fluid transfer, the release of energy is extremely fast and enables us to convert the slow input signal into exceptionally rapid events such as jumps. Last, our actuators can be simply reset and brought back to the initial configuration through vacuum and, therefore, can take off repetitively (see movie S6).

In this study, we have demonstrated the concept for spherical caps at the centimeter scale; however, our approach can be extended to any shape and does not depend on size. Because both  $\Delta E$  and the gravitational potential energy are proportional to the mass, the jump height is independent of size (34). Thus, we expect the relative jump,  $y_{\text{jump}} / R_i$ , to monotonically increase as the actuators are scaled down. On the other hand, on-board actuation and control may be embedded in larger jumpers (as the mass of these additional elements become negligible compared with that of the actuators) and open the way to real-world applications requiring untethered soft robots (35, 36). Last, in this work we have focused on the response of spherical caps under inflation; however, similar highly nonlinear behavior (i.e., force-displacement curves characterized by limit points in displacement) has been reported for the indentation of shallow arches (37) and shells with curved creases (38). Because structural elements with limit points in force have already been used to realize mechanical metamaterials with unique properties (39–43), we believe that by

integrating these new building blocks into their design, we can further expand their modes of functionality.

## MATERIALS AND METHODS

Details of the design, materials, and fabrication methods are summarized in sections S1 and S2. The experimental procedures, including the inflation with water to measure the pressure-volume curve and the inflation with air to measure jump height, are described in section S3. FE procedures and jumper mass-spring model are detailed in sections S4 and S5. Validation of the FE model and jumper mass-spring model is reported in section S6.

## SUPPLEMENTARY MATERIALS

robotics.sciencemag.org/cgi/content/full/5/42/eabb1967/DC1

Section S1. Design

Section S2. Fabrication

Section S3. Testing

Section S4. FE simulations

Section S5. Mass-spring model to predict the jump height

Section S6. Additional results

Fig. S1. Ideal design of the inflatable actuators.

Fig. S2. Manufacturable design of the inflatable actuators.

Fig. S3. Fabrication of the inflatable actuators.

Fig. S4. Baseline designs of the inflatable actuators.

Fig. S5. Experimental setup of the inflation with water.

Fig. S6. Experimental pressure-volume curves of the inflatable actuators.

Fig. S7. Experimental setup of the inflation with air.

Fig. S8. Jumping tests of the inflatable actuators.

Fig. S9. Effect of air compressibility.

Fig. S10. Numerical and experimental pressure-volume curves of the inflatable actuators.

Fig. S11. Pole displacement of the inflatable actuators.

Fig. S12. Three-dimensional simulations of the inflatable actuators.

Fig. S13. Axisymmetric simulations of the inflatable actuators.

Fig. S14. Extracting  $\Delta E$  from the numerical  $p$ - $v$  curves.

Fig. S15. Axisymmetric simulations of the inner cap.

Fig. S16. Asymmetric deformation emerges in designs with self-crossing pressure-volume curves.

Fig. S17. Axisymmetric simulations of the outer cap.

Fig. S18. Mass-spring model to predict jump height.

Fig. S19. Jump height prediction of the inflatable actuators.

Fig. S20. Validation of the spring-mass model.

Fig. S21. Improving the performance our soft fluidic actuators through a grid search.

Fig. S22. Influence of the outer cap stiffness on the actuators' response.

Movie S1. Snapping of spherical caps results in a sudden release of elastic energy.

Movie S2. Fast fluidic soft robots inspired by shell snapping.

Movie S3. Isochoric snapping enables jumping in fluidic soft robots.

Movie S4. Simplified mass-spring model to predict jump height.

Movie S5. Improving jumper design to increase jump height.

Movie S6. Inflatable actuator with repetitive jumping.

## REFERENCES AND NOTES

- D. Rus, M. T. Tolley, Design, fabrication and control of soft robots. *Nature* **521**, 467–475 (2015).
- C. Majidi, Soft robotics: A perspective—current trends and prospects for the future. *Soft Robot.* **1**, 5–11 (2014).
- D. Trivedi, C. D. Rahn, W. M. Kier, I. D. Walker, Soft robotics: Biological inspiration, state of the art, and future research. *Appl. Bionics Biomech.* **5**, 99 (2008).
- B. Gorissen, D. Reynaerts, S. Konishi, K. Yoshida, J. W. Kim, M. De Volder, Elastic inflatable actuators for soft robotic applications. *Adv. Mater.* **29**, 1604977 (2017).
- M. Runciman, A. Darzi, G. P. Mylonas, Soft robotics in minimally invasive surgery. *Soft Robot.* **6**, 423–443 (2019).
- P. Polygerinos, Z. Wang, K. C. Galloway, R. J. Wood, C. J. Walsh, Soft robotic glove for combined assistance and at-home rehabilitation. *Robot. Auton. Syst.* **73**, 135–143 (2015).
- E. Brown, N. Rodenberg, J. Amend, A. Mozeika, E. Steltz, M. R. Zakin, H. Lipson, H. M. Jaeger, Universal robotic gripper based on the jamming of granular material. *Proc. Natl. Acad. Sci. U.S.A.* **107**, 18809–18814 (2010).
- J. Barreiros, H. Claire, B. Peele, O. Shapira, J. Spjut, D. Luebke, M. Jung, R. Shepherd, Fluidic elastomer actuators for haptic interactions in virtual reality. *IEEE Robot. Autom. Lett.* **4**, 277–284 (2019).
- B. Mosadegh, P. Polygerinos, C. Keplinger, S. Wennstedt, R. F. Shepherd, U. Gupta, J. Shim, K. Bertoldi, C. J. Walsh, G. M. Whitesides, Pneumatic networks for soft robotics that actuate rapidly. *Adv. Funct. Mater.* **24**, 2163–2170 (2014).
- R. F. Shepherd, A. A. Stokes, J. Freake, J. Barber, P. W. Snyder, A. D. Mazzeo, L. Cademartiri, S. A. Morin, G. M. Whitesides, Using explosions to power a soft robot. *Angew. Chem. Int. Ed.* **52**, 2892–2892 (2013).
- J. T. Overvelde, T. Kloek, J. J. D'haen, K. Bertoldi, Amplifying the response of soft actuators by harnessing snap-through instabilities. *Proc. Natl. Acad. Sci. U.S.A.* **112**, 10863–10868 (2015).
- P. Rothmund, A. Ainla, L. Belding, D. J. Preston, S. Kurihara, Z. Suo, G. M. Whitesides, A soft, bistable valve for autonomous control of soft actuators. *Sci. Robot.* **3**, eaar7986 (2018).
- Y. Forterre, J. M. Skotheim, J. Dumais, L. Mahadevan, How the venus flytrap snaps. *Nature* **433**, 421–425 (2005).
- A. Pandey, D. E. Moulton, D. Vella, D. P. Holmes, Dynamics of snapping beams and jumping poppers. *EPL* **105**, 24001 (2014).
- D. Vella, Buffering by buckling as a route for elastic deformation. *Nat. Rev. Phys.* **1**, 425–436 (2019).
- H. Lee, C. Xia, N. X. Fang, First jump of microgel; actuation speed enhancement by elastic instability. *Soft Matter* **6**, 4342–4345 (2010).
- A. N. Gent, A new constitutive relation for rubber. *Rubber Chem. Technol.* **69**, 59–61 (1996).
- E. Riks, An incremental approach to the solution of buckling and snapping problems. *Int. J. Solids Struct.* **15**, 524–551 (1979).
- M. A. Crisfield, A fast incremental/iterative solution procedure that handles snap-through. *Comput. Struct.* **13**, 55–62 (1983).
- J. W. Hutchinson, Buckling of spherical shells revisited. *Proc. R. Soc. A* **472**, 20160577 (2016).
- A. Lee, F. L. Jiménez, J. Marthelot, J. W. Hutchinson, P. M. Reis, The geometric role of precisely engineered imperfections on the critical buckling load of spherical elastic shells. *J. Appl. Mech.* **83**, 111005 (2016).
- R. Zoelly, Ueber ein knickungsproblem an der kugelschale, thesis, ETH Zurich (1915).
- B. Florijn, C. Coulais, M. van Hecke, Programmable mechanical metamaterials. *Phys. Rev. Lett.* **113**, 175503 (2014).
- L. Stein-Montalvo, P. Costa, M. Pezulla, D. P. Holmes, Buckling of geometrically confined shells. *Soft Matter* **15**, 1215–1222 (2019).
- J. T. B. Overvelde, D. M. J. Dykstra, R. de Rooij, J. Weaver, K. Bertoldi, Tensile instability in a thick elastic body. *Phys. Rev. Lett.* **117**, 094301 (2016).
- A. Needleman, Inflation of spherical rubber balloons. *Int. J. Solids Struct.* **13**, 409–421 (1977).
- I. Müller, P. Strehlow, *Rubber and Rubber Balloons: Paradigms of Thermodynamics* (Springer Science & Business Media, 2004), vol. 637.
- M. Gomez, D. E. Moulton, D. Vella, Dynamics of viscoelastic snap-through. *J. Mech. Phys. Solids* **124**, 781–813 (2019).
- D. Karagiozova, X.-W. Zhang, T.-X. Yu, Static and dynamic snap-through behaviour of an elastic spherical shell. *Acta Mech. Sinica* **28**, 695–710 (2012).
- N. Vassios, A. J. Gross, S. Soifer, J. T. Overvelde, K. Bertoldi, Harnessing viscous flow to simplify the actuation of fluidic soft robots. *Soft Robot.* **7**, 1–9 (2019).
- B. Gorissen, E. Milana, A. Baeyens, E. Broeders, J. Christiaens, K. Collin, D. Reynaerts, M. De Volder, Hardware sequencing of inflatable nonlinear actuators for autonomous soft robots. *Adv. Mater.* **31**, 1804598 (2019).
- L. Hines, K. Petersen, M. Sitti, Inflated soft actuators with reversible stable deformations. *Adv. Mater.* **28**, 3690–3696 (2016).
- E. Ben-Haim, L. Salem, Y. Or, A. D. Gat, Single-input control of multiple fluid-driven elastic actuators via interaction between bistability and viscosity. *Soft Robot.* **7**, 259–265 (2019).
- S. Mahajan, *The Art of Insight in Science and Engineering: Mastering Complexity* (MIT Press, 2014).
- A. Rafsanjani, Y. Zhang, B. Liu, S. M. Rubinstein, K. Bertoldi, Kirigami skins make a simple soft actuator crawl. *Sci. Robot.* **3**, eaar7555 (2018).
- M. T. Tolley, R. F. Shepherd, B. Mosadegh, K. C. Galloway, M. Wehner, M. Karpelson, R. J. Wood, G. M. Whitesides, A resilient, untethered soft robot. *Soft Robot.* **1**, 213–223 (2014).
- R. M. Neville, R. M. Groh, A. Pirrera, M. Schenk, Shape control for experimental continuation. *Phys. Rev. Lett.* **120**, 254101 (2018).
- N. P. Bende, A. A. Evans, S. Innes-Gold, L. A. Marin, I. Cohen, R. C. Hayward, C. D. Santangelo, Geometrically controlled snapping transitions in shells with curved creases. *Proc. Natl. Acad. Sci. U.S.A.* **112**, 11175–11180 (2015).
- J. R. Raney, N. Nadkarni, C. Daraio, D. M. Kochmann, J. A. Lewis, K. Bertoldi, Stable propagation of mechanical signals in soft media using stored elastic energy. *Proc. Natl. Acad. Sci. U.S.A.* **113**, 9722–9727 (2016).

40. N. Nadkarni, A. F. Arrieta, C. Chong, D. M. Kochmann, C. Daraio, Unidirectional transition waves in bistable lattices. *Phys. Rev. Lett.* **116**, 244501 (2016).
41. S. Shan, S. H. Kang, J. R. Rane, P. Wang, L. Fang, F. Candido, J. A. Lewis, K. Bertoldi, Multistable architected materials for trapping elastic strain energy. *Adv. Mater.* **27**, 4296–4301 (2015).
42. T. Chen, O. R. Bilal, K. Shea, C. Daraio, Harnessing bistability for directional propulsion of soft, untethered robots. *Proc. Natl. Acad. Sci. U.S.A.* **115**, 5698–5702 (2018).
43. A. Rafsanjani, A. Akbarzadeh, D. Pasini, Snapping mechanical metamaterials under tension. *Adv. Mater.* **27**, 5931–5935 (2015).

**Funding:** Research was supported by the NSF grants DMR-1420570 and DMR-1922321 and the Fund for Scientific Research-Flanders (FWO). **Author contributions:** B.G. proposed the research idea. B.G., D.M., N.V., M.T., and K.B. developed the concept and

designed the research. D.M. conducted the numerical simulations. B.G. fabricated the prototypes. B.G. and D.M. performed the experiments. B.G., D.M., and K.B. postprocessed the data and wrote the paper. K.B. supervised the research. **Competing interests:** The authors declare that they have no competing interests. **Data and materials availability:** All data needed to evaluate the conclusions in the paper are present in the paper or the Supplementary Materials.

Submitted 6 February 2020  
Accepted 8 April 2020  
Published 20 May 2020  
10.1126/scirobotics.abb1967

**Citation:** B. Gorissen, D. Melancon, N. Vasios, M. Torbati, K. Bertoldi, Inflatable soft jumper inspired by shell snapping. *Sci. Robot.* **5**, eabb1967 (2020).

## Inflatable soft jumper inspired by shell snapping

Benjamin Gorissen, David Melancon, Nikolaos Vasios, Mehdi Torbati, and Katia Bertoldi

*Sci. Robot.* **5** (42), eabb1967. DOI: 10.1126/scirobotics.abb1967

### View the article online

<https://www.science.org/doi/10.1126/scirobotics.abb1967>

### Permissions

<https://www.science.org/help/reprints-and-permissions>

Use of this article is subject to the [Terms of service](#)

---

*Science Robotics* (ISSN 2470-9476) is published by the American Association for the Advancement of Science, 1200 New York Avenue NW, Washington, DC 20005. The title *Science Robotics* is a registered trademark of AAAS.

Copyright © 2020 The Authors, some rights reserved; exclusive licensee American Association for the Advancement of Science. No claim to original U.S. Government Works